Numerical study on the flexural capacity of ultra-light composite timber sandwich panels

Siavash Darzi [1]; Hassan Karampour [1,*]; Benoit P. Gilbert [1]; Henri Bailleres [2]

[1]Griffith School of Engineering and Built Environment, Griffith University, Gold Coast Campus, QLD 4222, Australia
[2]Salisbury Research Facility, Department of Agriculture and Fisheries, Salisbury, QLD 4107, Australia

Abstract:

The flexural stiffness and ultimate load capacity of novel ultralight composite sandwich panels, made of plywood faces and bamboo or peeling cores are investigated herein. Modified Ritz method and sandwich beam theory formulations for composite sandwich panels with thick faces and thick/stiff cores are developed, and are used to find the bending stiffness of the panels in one-way and two-way bending. The ultimate capacity and failure modes of the panels are then predicted from nonlinear material and geometric finite element analyses (FEA). The numerical methods are validated against published experimental results of orthotropic composite sandwich panels. It is shown that at similar panel depths, the proposed composite timber panels can be as high as 15% stiffer and 40% lighter than the existing commercial cross-laminated timber (CLT) panels. Results of a parametric study on selected composite panels with different yield stresses in compression, show that panels with bamboo cores exhibit relatively more ductile behaviour compared to those with peeling cores. At the ultimate flexural capacity, the tensile face of the panels fails in tension parallel to the grain, while the compressive face almost reaches its yield capacity.

Keywords: Ultra-light panel**;** Composite timber panel; Bamboo core; Ritz method; Sandwich beam theory; Cross-laminated timber (CLT); Cellular structures

1. Introduction

In structural engineering applications, sandwich panels are typically fabricated by attaching two thin and stiff skins, to a lightweight, flexible and relatively thick core. Sandwich panels are extensively used in automotive, aerospace, marine and industrial applications due to their high strength-to-weight and stiffness-to-weight ratios. Recently, there has been a growing trend in the construction industry to use sandwich structural elements for floors and load bearing walls [1]. Common skin materials include thin metal sheets [2], fibre reinforced polymer (FRP) composites [3], and in some structural applications, reinforced concrete [4]. Core materials include balsa wood [5], polymeric foams [6], Fibre Reinforced Polymer (FRP) cores [7], metallic foams [8,9], and honeycomb cells [10]. With recent changes in legislations and the growing trend towards tall mass-timber buildings, engineered wood products (EWP) such as Cross-laminated Timber (CLT) have gained increased popularity in residential and commercial construction in the form of slabs and load bearing walls. A CLT panel, (Fig. 1a.) is comprised of an odd number of orthogonally bonded layers of solid sawn lumbers, which are bonded using adhesive, nails or wooden dowels [11]. CLT is a lighter alternative compared to concrete and composite concrete-steel slabs and walls. However, CLT is susceptible to rolling shear failure [12], and the congestion of material in the vicinity of the neutral axis, reduces the efficiency of CLT panels in flexure. Unlike CLT, in a sandwich panel and with respect to bending characteristics, the material is efficiently distributed over the cross-section.

Most of the existing composite sandwich panels use low-strength material such as foam in the core component. In bending action, the role of the core is critical in transmitting the shear between the face in compression and the one in tension. Therefore, sandwich panels with soft cores are not optimal solution for structural members subject to bending actions such as slabs

[13]. To overcome this issue, several researchers have used high-density core material to improve the load bearing capacity of the sandwich structures. Daniel and Abot [14] filled the cells of a honeycomb core with epoxy to prevent premature shear failure of the composite sandwich panels. Codyre and Fam [15] showed that doubling and tripling the foam core density in sandwich panels with GFRP skins led to increases in peak load by 170%, due to the enhanced composite action and reduced shear deformations. Mahfuz et al. [16] improved the performance of composite sandwich panels under flexure by infusing titanium dioxide (TiO2) nanoparticles into the parent polyethylene foam material to strengthen the core structure. Their results showed that a 53% increase in the flexural strength could be attained by infusing 3% loading of TiO2 nanoparticles in the core. However, such advantages disappear as the floor spans become longer. Some researchers have proposed alternative forms for sandwich panels, by introducing FRP stitches through foam cores to improve the performance of the foam core [17,18]. The results show some improvements in the flexural response and the stitches prevent the de-bonding of the core from the faces.

The previously mentioned studies [16,17] showed that the enhancement of the core material significantly improves the performance of the composite sandwich panels. The drawback however, is that the weight and the production cost of these composite sandwiches are also significantly increased. To address these drawbacks, two novel lightweight sandwich panels, namely; (a) Bamboo Core Sandwich (BCS) panel, and (b) Peeling Core Sandwich (PCS) panel are proposed herein. The Bamboo Core Sandwich (BCS) panel is depicted in Fig. 1b and is comprised of vertically aligned hollow bamboo rings (core) and commercial plywood laminates (faces). The hollow bamboo rings are bonded to the face skins using a polyurethane structural adhesive. Bamboo is a light sustainable natural material, can be harvested in 3–4 years from the time of planting, is recyclable and has mechanical properties comparable to

those of conventional building materials [19]. The Peeling Core Sandwich (PCS) panel is shown in Fig. 1c. Similar to the BCS panel, the faces of the PCS panel are made from commercial plywood laminates. The core is made up of peeling cores, which are the unused products left from the wood log peeled into veneers in a lathe machine. Depending on the specifications of the veneer log peeling lathe machine, the peeling cores may have diameters of 40-120 mm [20].

In this paper, the flexural stiffness and ultimate strength of the proposed BCS and PCS panels under uniformly distributed transverse load are investigated using a proposed Ritz method and a validated FEA. In Section 2, a Ritz formulation (energy method), is developed that can capture the flexural stiffness of sandwich panels with thick cores, in one-way and two-way bending. The accuracy of the proposed Ritz-method is validated against published experimental results of a Glass Fibre Reinforced Polymer (GFRP) sandwich panel in two-way bending and, to the theoretical predictions of sandwich beam theory (Timoshenko beam theory) in one-way bending. Using the developed Ritz method, effects of the thickness and material properties of the plywood skins and height of the core, on the bending stiffness of the panels are discussed in Section 3. The Ritz method is preferred to the FEA due to its computational efficiency and is therefore used to carry out the parametric study on the stiffness of the panels. The results are compared to the bending stiffness of commercially available CLT panels of almost similar depths. In Section 4, the ultimate flexural strength and failure modes of the BCS and PCS panels are calculated using FEA with nonlinear geometric and material definitions.

2. Methodology and validation

2.1 The Ritz method

The flexural behaviour of the BCS and PCS panels under uniformly distributed loads, with two-edge simply supported (one-way bending) and four-edge simply supported (two-way bending) configurations is investigated using the Ritz method. To do so, a new formulation for bending of sandwich orthotropic plates with thick core/thick face under transverse deflection is derived. In this method, the total strain energy of the system, which consists of the in-plane and shear strains of the core, membrane, shear and local bending strains of the faces, is calculated. Small deflection theory is adopted and therefore, it is assumed that the middle plane of the orthotropic plate does not stretch under transverse deflections. Due to the difference in stiffness of the core compared to the plywood faces, the strain energy terms incorporate the shearing strain of the core in orthogonal directions and purely in-plane shearing strain of the faces. Unlike existing formulation for sandwich panels with soft cores, in derivation of the Ritz equations herein, the flexural rigidity of the cores of the BCS and PCS panels are not neglected. Also, to be able to extend the Ritz formulation to BCS and PCS panels with thick faces, the local bending stiffness of the faces are considered. By assuming an appropriate expression for the deflection of the orthotropic plate and considering the boundary conditions of the panels, the total energy of the system is obtained by adding the total strain energy of the deformed panel and the potential energy of the applied load. The deflected configuration that corresponds to the minimum total energy in the panel under assumed transverse load is obtained, and the corresponding mid-span deflection of the panel is calculated. The flexural stiffness of the BCS and PCS panel is obtained by finding the slope of the corresponding load-deflection curve. The problem formulation is discussed herein.

Displacements and Strains

Schematic view of the panels are shown in Fig. 1b and 1c. The load is assumed to be applied on the top face and in the positive z direction. The displacement in the x, y and z directions are denoted with u, v and w respectively. A section of the deflected panel parallel with the xz plane, after undergoing a displacement in the z direction is shown in Fig. 2. During the subsequent displacement, if there were no shear strains, the line $abcde$, which is normal to the centre line of the undeformed panel, would rotate through an angle $\partial w/\partial x$ to the position $a'b'c'd'e'$ and would remain normal to the centre line of the sandwich panel. In the BCS and PCS panels, the cores are not soft and contribute to the flexural rigidity of the composite panel. Therefore, the line $abcde$ moves to a new position $a"b"c'd"e"$ during the subsequent displacement. Since the shear strains in the faces are assumed to be negligible, the lines $a"b"$ and $d"e"$ remain parallel with $a'b'c'd'e'$. The angle $\widehat{d'c'd"}$ is equal to the shear strain γ and $\widehat{d"c'z}$ is denoted with λ $(\partial w/\partial x)$. The quantity λ may take any value between +1 and $-\frac{t}{c}$ (t<c), where c is the core height and t is the face thickness. The value $\lambda = +1$ applies when $\gamma = 0$ and the panel behaves as composite beam. The other extreme, $\lambda = -\frac{t}{c}$ represents a sandwich panel with a core so flexible in shear that cannot provide any connection between the two faces [21]. For an orthotropic plate, a similar diagram may be drawn for the yz plane (not shown here) to obtain the displacement in y direction. In this case, μ would be a parameter such that a line in the core, which is originally vertical, rotates in the yz plane through an angle μ $(\partial w/\partial y)$.

The displacements u and v in x and y directions of any point within the deformed sandwich panel and with respect to the notations presented in Fig. 2 can be obtained as follows:

Displacement field in the core

$$u_c = -z\lambda\frac{\partial w}{\partial x}, \quad -\frac{c}{2} \le z \le +\frac{c}{2} \tag{1a}$$

$$v_c = -z\mu\frac{\partial w}{\partial y}, \quad -\frac{c}{2} \le z \le +\frac{c}{2} \tag{1b}$$

Displacement field in the lower face

$$u_f = -\frac{c}{2}\lambda\frac{\partial w}{\partial x} - \left(z - \frac{c}{2}\right)\frac{\partial w}{\partial x} = -\left\{\frac{c}{2}(\lambda - 1) + z\right\}\frac{\partial w}{\partial x}, \quad \frac{c}{2} \le z \le \frac{h}{2} \tag{2a}$$

$$v_f = -\left\{\frac{c}{2}(\mu - 1) + z\right\}\frac{\partial w}{\partial y}, \quad \frac{c}{2} \le z \le \frac{h}{2} \tag{2b}$$

Displacement field in the mid-plane of the lower face

$$u_{fm} = -\frac{1}{2}(c\lambda + t)\frac{\partial w}{\partial x}, \quad z = \frac{c+t}{2} \tag{3a}$$

$$v_{fm} = -\frac{1}{2}(c\mu + t)\frac{\partial w}{\partial y}, \quad z = \frac{c+t}{2} \tag{3b}$$

where h is the overall depth of the panel as shown in Fig. 2. The expressions for the strains are obtained by differentiation of the above displacements u and v within the corresponding displacement fields. The longitudinal strains $\in$ and shear strains γ in the core are

$$\in_x^c = \frac{\partial u}{\partial x} = -z\lambda\frac{\partial^2 w}{\partial x^2} \tag{4a}$$

$$\in_y^c = \frac{\partial v}{\partial y} = -z\mu\frac{\partial^2 w}{\partial y^2} \tag{4b}$$

$$\gamma_{zx}^c = \frac{\partial u}{\partial z} + \frac{\partial w}{\partial x} = (1 - \lambda)\frac{\partial w}{\partial x} \tag{4c}$$

$$\gamma_{yz}^{c}=\frac{\partial v}{\partial z}+\frac{\partial w}{\partial y}=(1-\mu)\frac{\partial w}{\partial y} \tag{4d}$$

$$\gamma_{xy}^{c}=\frac{\partial u}{\partial y}+\frac{\partial v}{\partial x}=-z(\lambda+\mu)\frac{\partial^2 w}{\partial x\partial y} \tag{4e}$$

The strains in the faces consist of the longitudinal membrane strains $\in^{fm}$, shear membrane strains γ^{fm}, and local bending strains $\in^{fL}$.Membrane strains at the middle plane of the faces are obtained by differentiation of Eqs. 3a and 3b

$$\in_{x}^{fm}=\frac{\partial u}{\partial x}=-\frac{1}{2}(c\lambda+t)\frac{\partial^2 w}{\partial x^2} \tag{5a}$$

$$\in_{y}^{fm}=\frac{\partial v}{\partial y}=-\frac{1}{2}(c\mu+t)\frac{\partial^2 w}{\partial y^2} \tag{5b}$$

$$\gamma_{xy}^{fm}=\frac{\partial u}{\partial y}+\frac{\partial v}{\partial x}=-\frac{\partial^2 w}{\partial x\partial y}\left(\frac{c}{2}\lambda+\frac{c}{2}\mu+t\right) \tag{5c}$$

The *x* displacement of any point *z* in the lower face with respect to the middle plane of the lower face is

$$u_{fL}=-\left\{\frac{c}{2}(\lambda-1)+z\right\}\frac{\partial w}{\partial x}+\frac{1}{2}(c\lambda+t)\frac{\partial w}{\partial x}=-\left(z-\frac{c}{2}-\frac{t}{2}\right)\frac{\partial w}{\partial x} \tag{6a}$$

$$v_{fL}=-\left\{\frac{c}{2}(\mu-1)+z\right\}\frac{\partial w}{\partial y}+\frac{1}{2}(c\mu+t)\frac{\partial w}{\partial y}=-\left(z-\frac{c}{2}-\frac{t}{2}\right)\frac{\partial w}{\partial y} \tag{6b}$$

The corresponding local bending strains and shear strain in the lower face are

$$\in_{x}^{fL}=-\left(z-\frac{c}{2}-\frac{t}{2}\right)\frac{\partial^2 w}{\partial x^2},\quad \frac{c}{2}\le z\le\frac{h}{2} \tag{6c}$$

$$\in_y^{fL} = -\left(z - \frac{c}{2} - \frac{t}{2}\right)\frac{\partial^2 w}{\partial y^2}, \quad \frac{c}{2} \le z \le \frac{h}{2} \tag{6d}$$

$$\gamma_{xy}^{fL} = \frac{\partial u}{\partial y} + \frac{\partial v}{\partial x} = -2\left(z - \frac{c}{2} - \frac{t}{2}\right)\frac{\partial^2 w}{\partial x \partial y} \tag{6e}$$

The total direct strain in the faces is calculated by adding the membrane and local bending strains. The total direct strain in the lower face in x direction $\in_x$ is the sum of the Eqs. 5a and 6c, and in the y direction $\in_y$ is the sum of Eqs. 5b and 6d.

Energy equation

The strain energy per unit volume of the faces U_f is calculated by adding the total strain energy and shear strain energy of the lower and upper faces

$$U_f = 2\left[\frac{1}{2g}\int_V \left\{E^f{}_x \in_x^2 + E^f{}_y \in_y^2 + 2E^f{}_x \nu^f{}_{yx} \in_x \in_y\right\} dV + \frac{1}{2}\int_V \left\{G^f{}_{zx}\gamma_{zx}^2 + G^f{}_{xy}\gamma_{xy}^2 + G^f{}_{yz}\gamma_{yz}^2\right\} dV\right] \tag{7}$$

where E_x, E_y are the elastic moduli, G_{xy}, G_{yz}, G_{xz} are the shear moduli and υ_{xy}, υ_{yx} are the Poisson's ratios of the faces. $\in_x$ and $\in_y$ are the total direct strains in the lower face in x and y directions and $g = (1 - \upsilon_{xy}\upsilon_{yx})$. The factor of two in Eq. 7 accounts for the strain energy of the upper face. It should be noted that, when the plywood faces are shallow in proportion to their spans, the shear strain energy in zx and yz planes can be neglected. Similarly, the strain energy per unit volume of the core U_c is obtained by adding the longitudinal and shear strain energies, obtained from the strain expressions defined in Eq. 4:

$$U_c = \frac{1}{2g}\int_V \left\{ E^c{}_x \left(-z\lambda \frac{\partial^2 w}{\partial x^2} \right)^2 + E^c{}_y \left(-z\mu \frac{\partial^2 w}{\partial y^2} \right)^2 + 2E^c{}_x \nu^c{}_{yx} \left(-z\lambda \frac{\partial^2 w}{\partial x^2} \right)\left(-z\mu \frac{\partial^2 w}{\partial y^2} \right) \right\} dV + \frac{1}{2}\int_V \left\{ G^c{}_{zx} \left((1-\lambda)\frac{\partial w}{\partial x} \right)^2 + G^c{}_{xy} \left(-z(\lambda+\mu)\frac{\partial^2 w}{\partial x \partial y} \right)^2 + G^c{}_{yz} \left((1-\mu)\frac{\partial w}{\partial y} \right)^2 \right\} dV \quad (8)$$

Unlike previous studies with flexible core materials which neglect the core stiffness, Eq. 8 includes the in-plane stiffness of the core. The shear stiffness in the xy plane of the core is also considered in the present model. The strain energy due to direct stresses and strains in the z direction is neglected due to high stiffness of the core materials in z direction (low possibility of significant flattening or squashing) and small intensity of the transverse load.

The numerical integrations in Eqs. 7-8 are carried out over the volume of the face and core respectively. The numerical integration of Eq. 7 (in the faces) is straightforward, because the volume of the faces does not change in the xy plane. However, the in-plane (xy plane) cross-sectional areas of the bamboo and peeling cores vary across the panel. To simplify the numerical integration of Eq. 8, the factors K_B and K_P are introduced to define the ratio of the core material to the total volume of the core, in the BCS and PCS panels, respectively. These factors are multiplied by the modulus of elasticity and shear modulus of the core in Eq. 8.

$$K_B = \left[\frac{\pi\left(R^2 - r^2\right) \times c}{abc} \right] \times n \quad (9a)$$

$$K_P = \left[\frac{\pi D^2 \times c}{4abc} \right] \times n \quad (9b)$$

where R and r are the outer radius and inner radius of the hollow bamboo sections, respectively and D is the diameter of the peeling core. The total number of bamboo rings or peeling cylinders within the panel with length of a and width of b is equal to n.

Total potential energy

The change of potential energy associated with the deformation of the orthotropic sandwich plate under uniform transverse load q_{uni} is

$$V = -\int_0^a \int_0^b w q_{uni} dxdy = -q_{uni} \int_A w dA \tag{10}$$

The load q_{uni} can be represented by a double Fourier series expansion

$$q_{uni} = \sum_{m=1}^{\infty}\sum_{n=1}^{\infty} \frac{16q}{\pi^2 mn} \sin\left(\frac{m\pi x}{a}\right)\sin\left(\frac{n\pi y}{b}\right) \tag{11}$$

where a and b are the length and width of the panel shown in Fig. 1. A point load can be regarded as a local pressure applied over a small rectangular area with length a' and width b', at the centre of the panel located at (ψ, η)), and can be shown in following double Fourier series format

$$q_{point} = \sum_{m=1}^{\infty}\sum_{n=1}^{\infty} \frac{16P}{\pi^2 mna'b'} \sin\left(\frac{m\pi\psi}{a}\right)\sin\left(\frac{n\pi\eta}{b}\right)\sin\left(\frac{m\pi a'}{2a}\right)\sin\left(\frac{n\pi b'}{2b}\right)\sin\left(\frac{m\pi x}{a}\right)\sin\left(\frac{n\pi y}{b}\right)$$

(12)

To thoroughly validate the method for the one-way and two-way bending deformations of the panels, two-edge simply supported and four-edge simply supported boundary conditions are adopted. Knowing that deflection and bending moments vanish at the simply supported edges, the following expressions for the deflected shapes are assumed for the two-way bending (four-edge simply supported)

$$w = \sum_{m=1}^{\infty}\sum_{n=1}^{\infty} a_{mn} \sin\left(\frac{m\pi x}{a}\right)\sin\left(\frac{n\pi y}{b}\right) \tag{13}$$

$$w=0,\quad \frac{\partial^2 w}{\partial x^2}=0 \quad \text{at} \quad x=0 \ \text{and} \ x=a$$
$$w=0,\quad \frac{\partial^2 w}{\partial y^2}=0 \quad \text{at} \quad y=0 \ \text{and} \ y=b \tag{13a}$$

and for the one-way bending (two-edge simply supported)

$$w=\sum_{m=1}^{\infty} a_m \sin\left(\frac{m\pi x}{a}\right) \tag{14}$$

$$w=0,\quad \frac{\partial^2 w}{\partial x^2}=0 \quad \text{at} \quad x=0 \ \text{and} \ x=a \tag{14a}$$

where a_{mn} is the deflection amplitude at the middle of the panel ($x = a/2$, $y = b/2$). The total energy of system $\Pi = U_f + U_c + V$ and is equal to the summation of Eqs.7, 8 and 10. Π is a function of a_{mn}, λ and μ. In the Ritz method, the stable deflected shape corresponds to the values of a_{mn}, λ and μ , which minimise the total energy Π. These values are calculated by solving the following system of equations in MATLAB [22]

$$\frac{\delta}{\delta\lambda}(\Pi)=0$$
$$\frac{\delta}{\delta\mu}(\Pi)=0 \tag{15}$$
$$\frac{\delta}{\delta a_{mn}}(\Pi)=0$$

2.2 Sandwich beam theory

Narrow BCS and PCS panels act in one-way bending under transverse loads. Therefore, deflections of such panels can be approximated using Timoshenko beam theory [23]. The model takes into account rotational bending and shear deformation effects. The total elastic

displacement of the mid-span of a simply supported narrow sandwich panel (Δ) is the sum of flexural (w_1) and shear (w_2) deformations:

$$\Delta = w_1 + w_2 = \frac{5a^4 q}{384(EI)_{eq}} + \frac{a^2 q\kappa}{8(AG)_{eq}} \tag{16}$$

where q is the uniformly distributed load, $(EI)_{eq}$ and $(AG)_{eq}$ are the equivalent flexural and shear rigidities, respectively, and κ is the Timoshenko shear coefficient. The flexural rigidity of the BCS or PCS narrow panels is the sum of the bending rigidities of the plywood faces and the bamboo/peeling cores

$$(EI)_{eq} = 2\times E_f \frac{bt^3}{12} + 2\times E_f bt\left(\frac{d}{2}\right)^2 + E_c \frac{(b_c)c^3}{12} \tag{17}$$

where E_f and E_c are the elastic modulus of the plywood faces and the core in the span direction, respectively. The width of the faces and the core are represented by b and b_c in Eq. 16, respectively. In the BCS panel at any given cross-section cut along the span (parallel to the yz plane in Fig. 1b), b_c is almost equal to $2en_{yz}$, where e is the bamboo wall-thickness and n_{yz} is the number of bamboos across the width of the panel (Fig. 1b). In the PCS panel, the width of the core (b_c) varies along the span at various x-coordinates. A cut-through single peeling core (parallel to the yz plane) of the PCS panel is depicted in Fig. 3a. Since the third term in Eq. 17 corresponds to the flexural rigidity of the core, it is meaningful to find an equivalent core width b_c, based on the moment of inertia of the peeling core at the cut-section.

$$b_c = 2R\ n_{yz}\frac{I_\xi}{\bar{I}_\xi}$$

$$\bar{I}_\xi = \frac{1}{12}(2Rc^3) \tag{18}$$

$$I_\xi = \frac{1}{R}\int_0^R \frac{c^3}{12} D_\xi d\xi = \frac{1}{R}\int_0^R \frac{c^3}{12}\left(2R\sqrt{1-\left(1-\frac{\xi}{R}\right)^2}\right)d\xi$$

where D_ξ is the thickness of a peeling core (Fig. 3a), cut at distance ξ away from an edge, and n_{yz} is the number of peeling cores with radius R, along the width of the PCS panel (Fig. 1c). The deformation due to shear (w_2 in Eq. 16), is calculated with respect to a tilted deformed section of the narrow panel shown in Fig. 3b. The shear strain γ is assumed to be constant through the core height. Under a transverse load, the faces and the longitudinal centre-line of the narrow panel tilt, and the relation between the slope of the panel $\frac{\partial w_2}{\partial x}$ and the core shear strain γ is obtained from Fig. 3b. As seen in the diagram $\gamma c = cf = de$. Hence

$$\frac{\partial w_2}{\partial x} = \gamma \times \frac{c}{d} = \frac{\tau}{G} \times \frac{c}{d} \tag{19}$$

For a composite panel the shear stress can be expressed as [21]

$$\tau = \frac{Q}{(EI)_{eq} b_c}\sum S_i.E_i \tag{20}$$

where $(EI)_{eq}$ is the flexural rigidity of the entire section (Eq. 17), S_i and E_i represent the first moment of area and modulus of elasticity of the face or the core, and Q is the shear force at the section. By substituting $(EI)_{eq}$ from Eq. 17 and γ from Eq. 19, into Eq. 20, the shear stress at any point within the core, at a distance z from the centre of the core is

$$\tau = \frac{Q}{(EI)_{eq}(b_c)}\left\{E_f \frac{btd}{2} + \frac{E_c(b_c)}{2}\left(\frac{c^2}{4} - z^2\right)\right\} \tag{21}$$

The shear stress distribution in the core is assumed to be constant and equal to average of the shear stress at the bottom of the face ($z = c/2$) and shear stress at the centre of the core ($z = 0$). Thus, the shear rigidity of the core and corresponding Timoshenko shear coefficients for BCS and PCS panels are

$$\begin{aligned} (AG)_{eq} &= (b_c d)G_c \\ \kappa &= \frac{c}{(EI)_{eq}}\left(E_f \frac{btd}{2} + \frac{E_c(b_c)}{4}\left(\frac{c^2}{4}\right)\right) \end{aligned} \tag{22}$$

It should be noted that most of CLT floor slabs have dimensions of proportion $a/b > 2$ (Fig. 1a), and are thus assumed to exhibit one-way bending. The same Timoshenko beam formulation (Eq. 16) known as the shear analogy method [24], is widely used in practice to calculate the deflection of the CLT panels. The flexural and shear rigidities of the CLT panel are

$$\begin{aligned} (EI)_{eff} &= \sum_{i=1}^{n} E_i.b_i.\frac{h_i^3}{12} + \sum_{i=1}^{n} E_i.A_i.z_i^2 \\ (AG)_{eff} &= \frac{d_a{}^2}{\left[\left(\frac{h_1}{2.G_1.b}\right) + \left(\sum_{i=2}^{n-1}\frac{h_i}{G_i.b_i}\right) + \left(\frac{h_n}{2.G_n.b}\right)\right]} \end{aligned} \tag{23}$$

where E_i is the modulus of elasticity and b_i and h_i are the width and thickness of each individual layer, respectively. z_i is the distance between the centre axis of each individual layer and the neutral axis of the entire cross-section of the CLT panel (Fig. 1a). G_i and A_i are the shear modulus and the area of cross-section of each individual layer, d_a is the distance

between the two centre axes of the top and bottom layers of the entire cross-section. h_n and G_n are the thickness and the shear modulus of the surface layer, respectively. The Timoshenko shear coefficient of CLT panel κ is equal to 1.2 [25].

2.3 Validation of the Ritz and the Sandwich beam theory methods

2.3.1 One-way bending

The flexural responses of BCS and PCS narrow panels in one-way bending under uniformly distributed load, from the Ritz method (Section 2.1) and the sandwich beam theory (Section 2.2) are compared in Fig. 4a. To do so, double layer BCS and PCS panels with length of 6 m and width of 1 m are considered. The panels are consisted of plywood ID 21-30-9 (described in Section 3.1) with a total thickness of 42 mm, and core depth of 200 mm. The outer radius of the bamboo and peeling cores (R) are 50 mm and the wall-thickness of bamboo (e) is 10 mm. The material properties of the core materials and plywood faces are represented in Table 1 and Table 2, respectively. As shown in Fig. 4a, the results from the proposed Ritz method and the sandwich beam theory almost coincide.

2.3.2 Two-way bending

The Ritz method proposed in Section 2.1 is validated against experimental results of a square 600×600 mm Glass Fibre Reinforced Polymer (GFRP) orthotropic sandwich panel reported in [26]. The sandwich panel used in the experimental study [26] is shown in Fig. 4b, and is made of glass fibre composite faces with wall thickness of 3 mm and a toughened phenol formaldehyde resin core with depth of 12 mm. The orthotropic material properties of the GFRP faces are represented in Table 1. The isotropic core has a modulus of elasticity 1,350 MPa and shear modulus of 746 MPa. In the experimental study, the panel was simply supported on four sides using steel screws that fixed the GFRP sandwich slab to the timber

(two-way bending). A point load was applied via a 100×100 mm steel plate, positioned at the centre of the panel. The load-deflection responses of the GFRP slab from the experimental results and the proposed Ritz method are presented in Fig. 4b. A reasonable correlation is observed between the Ritz method and the experimental results within the linear region. The difference between stiffness found from the experimental test and the Ritz method is less than 4%.

3. Flexural stiffness of the BCS and PCS panels in one-way and two-way bending

A parametric study is carried out in this section to investigate the influence of face thickness (t) and core height (c), on the flexural stiffness of the BCS and PCS panels in one-way (two-edge simply supported) and two-way (four-edge simply supported) bending. The flexural stiffness of the panels are obtained using the proposed Ritz method (Section 2.1), and are compared against those of CLT panels with almost identical depths, using the sandwich beam theory (shear analogy method), defined in Section 2.2.

3.1 The labelling scheme and the material properties of the panels

In the study that follows, three different structural plywood IDs are adopted for the faces of the panels, based on standard structural plywood construction in Australian/New Zealand standard [27]. The selected plywood IDs are 18-30-7, 21-30-9 and 25-30-9. The numbering sequence in the ID gives, the nominal plywood thickness, the face veneer thickness multiplied by 10, and the number of plies in the assembly. For instance, Plywood ID 18-30-7 in Table 2, describes 18 mm thick plywood, made of 3 mm thick veneers on the top and bottom plies, and total number of 7 plies. The nominal thickness of individual plies through the assembly is listed in Table 2. To increase the flexural stiffness of the panels, two plywoods of the same ID are glued together to construct the faces of the panels. Such panels are noted as double layer BCS/PCS panels herein. The double layer BCS/PCS panels have

the same core depth as the single layer panels. For instance, to make a double layer BCS 18-30-7 panel, plywoods with nominal thickness of 18 mm, face veneer thickness of 3 mm, made of 7 plies are glued to the top and bottom faces of the single layer BCS 18-30-7 panel. Therefore, a double layer BCS 18-30-7 panel consists of plywood faces of 36 mm with 14 plies. It should be noted that in classical sandwich panel theory, panels with $d/t < 5.77$ are categorised as sandwich panels with thick faces and those with $5.77 < d/t < 100$ are considered thin face ($d = c + t$). All the single and double layer BCS/PCS panels used in this study have $5.77 < d/t < 14.89$, which suggest that the proposed BCS/PCS panels have relatively thick faces. The outer radius of the bamboo and peeling cores are 50 mm and the wall-thickness of bamboo is 10 mm in all the models. The material properties of the core materials and plywood plies in BCS and PCS panels are shown in Table 1. The x, y and z directions correspond to the longitudinal (parallel to fibres), tangential and radial direction, respectively. The plywood plies are assumed to be made of plantation pine (*Pinus Radiata*) and the material properties are taken from [28]. The properties of bamboo are taken as the average values of *Moso* bamboo (*Phyllostachys pubescens*) reported in [29]. To find the mechanical properties of the plywood faces from orthotropic properties of each ply (*Radiata* plies), the *OSULaminates* tool, which is a *Java* application developed by *Oregon State University* for analysis of laminated plates [30] is utilised. *OSULaminates* uses classical laminate theory [31] to calculate the axial and bending rigidity of a laminated plate based on the properties of its individual layers. The material properties of the plywood laminate faces obtained by *OSULaminate*, comprised of *Radiata* plies with properties listed in Table 1, are presented in Table 2.

For sake of comparison, two commercial CLT panels, *CL7/295* and *CL7/315* are selected from *XLam* CLT products [31]. The *CL7/295* and *CL7/315* panels consist of seven layers of

sawn boards with a total thickness of 295 mm and 315 mm, respectively. The two outermost layers (1 and 7) and the middle layers (3 and 5) shown in Fig. 1a, are aligned in the span direction, and other layers are perpendicular to the span direction. The material properties of the CLT panel laminations are represented in Table 3 and are taken from *XLam* design guide [32].

3.2. Flexural stiffness of the narrow panels (one-way bending)

Flexural responses of the BCS and PCS panels in one-way bending under a uniformly distributed load of 5 kPa are investigated using the Ritz method. The panels have lengths of 4, 6 and 7 meters (a in Fig.1), width of 1 meter (b in Fig. 1), and are simply supported at either ends (at x=0 and x=a in Fig. 1). To study the effect of face thickness and core depth on the flexural response of the BCS panels in one-way bending, different BCS 18-30-7 panels are examined. Results of the mid-span deflection (Δ) of the panels with spans of 4, 6 and 7 meters, and under a uniformly distributed load of 5 kPa are plotted against the core depth (c) in Fig. 5. As shown in Fig. 5, the mid-span deflections of the double layer panels are much lower than the single layer panels of the same core depth (c). The differences in the mid-span deflections are more noticeable in longer spans. In addition, it is evident from Fig. 5 that the mid-span deflection of the double layer panels are less sensitive to the core depth (c), compared to the single layer panels.

Mid-span deflection versus the total depth (h) of the BCS panels with different face configurations, namely; BCS 18-30-7, BCS 21-30-9 and BCS 25-30-9 and under a uniformly distributed load of 5 kPa are presented in Fig. 6. The data points shown in black and red correspond to the single layer and double layer BCS panels, respectively. The target deflections for the BCS panels are shown with the dashed lines in each curve, and correspond

to the deflection of *CL7/295* in the 4 and 6 m panels, and to the deflection of *CL7/315* in the 7 m panel under 5 kPa uniformly distributed load. To reach the target deflection, total depth of the single layer BCS panel ($h = 2t + c$) is enlarged by increasing the core height (c). As shown in Figs. 6a, b and c by increasing the core height, the deflection of the single layer BCS panel is reduced. However, deflections of the single layer BCS panels only get smaller than the CLT panel, when the depth of the BCS panel exceeds the depth of the target CLT panel. Optimal results are obtained in double layer BCS panels (red data points in Fig. 6). The minimum deflections correspond to the double layer BCS 21-30-9 panels. At almost similar deflections, the depth (h) of the BCS 21-30-9 panel is 4% lower than the CLT panel (*CL7/295*) in 4 and 6m spans, and 7% lower smaller than the depth of the CLT panel (*CL7/315*) in the 7 m span. This ideal result is associated with the higher MOE of the faces of the double layer BCS 21-30-9 panel in the longitudinal direction, as represented in Table 2.

In Figs. 7a-7c, mid-span deflections of the BCS 21-30-9 panels are compared against PCS panels of similar specifications and are benchmarked against their commercial CLT competitors. Regardless of the span lengths, the PCS 21-30-9 panel exhibits smallest deflections. At similar panel depth of h =284 mm, the deflection of the PCS 21-30-9 panels are 16%, 10% and 8% lower than the BCS 21-30-9 panels, in 4, 6 and 7 m spans, respectively.

Shear to flexure deformation ratios (w_2/w_1) of BCS 21-30-9, PCS 21-30-9 and CL7/295 panels in one-way bending and under a uniform distributed load of 5 kPa are shown in Fig. 8. Contribution of shear and flexure in total deformation of the panels in one-way bending are calculated using the beam sandwich theory (Section 2.2). As shown in Fig. 8, at small aspect ratios (a/b<2), there is significant shear contribution. This is more evident in the CLT and BCS panels. At larger aspect ratios (a/b>5), the shear contributions almost vanish. In the PCS

panel, the w_2/w_1 is consistently smaller than one, and becomes negligible at $a/b>3$. The Timoshenko beam coefficients of the BCS and PCS panels are 0.817 and 0.815, respectively, and are much smaller than the coefficient 1.2 of the CLT panels. Using the Ritz method, in one-way bending, the shear angle factor λ (see Section 2.1), are found to be between 0.77-0.95 in the BCS panels, and between 0.92-0.98 in the PCS panels. It can be construed that due to the high stiffness of the peeling cores, the shear strain γ of the PCS cores, are almost equal to zero and thus, the panels behave similar to a composite panel.

3.3. Flexural stiffness of the wide panels (two-way bending)

Two-way flexural behaviour of the proposed sandwich panels under a 5 kPa uniformly distributed load is investigated, by modelling 6×8 m panels with three different face configurations (similar to narrows panels), by means of the Ritz method. Mid-span deflections of the BCS and CLT panels (deflection at the centre of the panel) are plotted against the corresponding panel depths in Fig. 9a. Similar to the one-way bending response, the double layer BCS 21-30-9 panel yields the optimum results. At the target deflection (7.64 mm), the depth of the double-layer BCS 21-30-9 panel is 4% smaller than the *CL7/295* panel.

Mid-span deflections of the BCS panels in two-way bending are compared against the PCS panels in Fig. 9b. Single layer PCS 21-30-9 and PCS 25-30-9 panels show smaller deflections compared to the single-layer BCS 21-30-9 panel. However, the optimum results in two-way bending is obtained by using double layer PCS 18-30-7 panel. At the target deflection (7.64 mm), panel depth of the double layer PCS 18-30-7 is h=272 mm, compared to h=295 mm in the *CL7/295* panel. In two-way bending, the BCS panels have shear angle factors λ and μ between 0.86-0.97 and 0.90-0.98, respectively. The λ and μ factors in the PCS panels, under two-way bending range between 0.96 and 0.99.

3.4 Efficiency of the BCS and PCS panels in comparison with the CLT panels

Geometric properties of the BCS and PCS panels, commercial CLT panels and their corresponding deflections, weight and stiffness ratios are represented in Table 4. The deflections of the CLT panels are calculated based on the sandwich beam theory (shear analogy method) and are compared with the deflections of selected BCS/PCS panels obtained from the Ritz method. Due to their optimal flexural behaviour, double layer BCS 21-30-9, double layer PCS 18-30-9 and double layer PCS 21-30-9 panels are selected. The stiffness of the panel (K) in Table 4 is calculated by inversing the mid-span deflection of the panel under the uniformly distributed load.

As represented in Table 4, in one-way bending ($a/b>2$), the BCS panel has stiffness between 6-17% higher than the CLT panel. The ratio between the stiffness of the CLT and the BCS panels, varies with the corresponding change in the aspect ratio (a/b). This is due to the fact that, in smaller aspect ratios, the contribution of the shear deformation (w_2 in Fig. 8) is more significant in CLT, which makes it less efficient compared to the BCS panel. As the aspect ratio (a/b) becomes larger, the shear contribution is decreased and the difference between stiffness of CLT and BCS panels becomes less significant. The stiffness of the PCS panels are larger than the CLT panels at all aspect ratios in one-way bending. A 25% increase in stiffness is obtained in PCS 21-30-9 with aspect ratio of 6, compared to the CLT. In two-way bending (6×8 m panel), the stiffness of the BCS and PCS panels are about 20% and 30% larger than the CLT. The panel depth of PCS 18-30-7 is 4% lower than BCS 21-30-9 panel, and 8% lower than the CLT panel.

The selected BCS and PCS panels represented in Table 4, weigh about 40% and 20% less than the CLT panel, respectively. The BCS panels are in average 23% lighter than the PCS

panels. In the BCS panels, the weight of the core is 85% of the weight of the faces. On the other hand, in the PCS panels, the core weighs almost twice the faces. This suggests that the BCS panels are the favourable sandwich products in terms of the material used in the core compared to the PCS panels.

4. Ultimate strength of the BCS and PCS panels

4.1 Finite Element model and validation

The ultimate flexural capacity of the BCS and PCS panels are studied using the commercial finite element analysis (FEA) software, ANSYS 17.0 [33]. The FE model is validated against the experimental results of the 600×600 mm Glass Fibre Reinforce Polymer (GFRP) sandwich panel, reported in [26] and discussed in Section 2.3. Orthotropic-elastic and isotropic elastic material properties are adopted for the GFRP faces and the modified phenolic core, respectively in the FEA. These are meshed with eight-node solid elements. The core and GFRP faces are bonded using no slippage contact definition in the FEA. The orthotropic material properties of the GFRP faces are represented in Table 1 and the isotropic core properties are reported in Section 2.3. Due to symmetry, only a quarter of the panel is modelled and simply supported boundary conditions are imposed on the edges. Uniform pressure is gradually applied over a $100 \times 100 \times 1$ mm steel plate (E =200 GPa) at the centre of the panel, similar to the loading procedure in the test [26]. The FEA result using nonlinear geometric analysis is shown in Fig. 4b, and is in a good agreement with the experimental results.

Using the validated FEA, double layer BCS 21-30-9 and PCS 21-30-9 panels, with dimensions of 6×1 m are modelled. The height of the bamboo and peeling cores are 200 mm and the total panel depth is 284 mm. The wall-thickness of the bamboo cores are 10 mm

and the radius of the bamboo and peeling cores are 50 mm. Eight-node solid 186 elements [33], with three degrees of freedom at each node are utilised to model the plywood veneers and the bamboo/ peeling cores. A schematic view of a short length of the FE mesh of the BCS and PCS panels are shown in Fig. 10a. Perfect bond contact definitions are adopted to model the contact between the plywood veneers, and between the cores and the faces. To account for the possible contact between the faces of the bamboo or peeling cores, bonded contact is defined between the core faces. Based on results from a convergence study, the faces and the cores are discretised with element length of 20 mm. Plywood veneers have one element along the veneer thickness, and the bamboo and the peeling cores are discretised with two and eight elements along the thickness, respectively (Fig. 10a). Using symmetry, only a quarter of the panel (3×0.5 m) is modelled in the FEA, and simply supported and symmetry conditions are imposed on the edges.

4.2 Material properties and failure criteria

The elastic material properties of bamboo, peeling core and *Radiata* ply veneers used in the FEA, are similar to those adopted in the Ritz method and are represented in Table 1. The x, y and z directions correspond to the longitudinal (parallel to the fibres), tangential and radial directions, respectively. The material properties are assigned to the PCS and BCS panels in the FEA, using a *Cartesian* coordinate system and to the cores via a *cylindrical* coordinate system. The bamboo/peeling cores are deemed to remain in the elastic region and thus, orthotropic elastic material definition is assumed in the cores. Material properties of the core are assumed to be identical in radial and tangential directions (transverse isotropic behaviour), as represented in Table 1.

In tension, the behaviour of timber is rather brittle [34] and the capacity in the direction perpendicular-to-grain ( ) is much lower than in the direction parallel-to-grain (וו). The maximum normal stress criterion, which is an acceptable failure criterion for anisotropic brittle materials [35], is adopted for the failure of *Radiata* in tension (the face in tension). The timber is assumed to fail in tension when any one of the stresses in the principal material directions exceeds the material strength in that direction. This assumes that failure is independently controlled by each stress type and it is not a function of interaction between stresses. A schematic view of the material definition in tension is shown in Fig. 10b. The timber tensile strength values are adopted in the FEA: $\sigma_{tu}^{\shortparallel}$ =27 MPa, and σ_{tu} =0.5 MPa [36, 37]. It should be noted that the variability of wood is high and the determination of values can influence the results of simulation.

In compression, timber exhibits relatively ductile behaviour [34] which can be represented with elastic-plastic material constitutive laws. To account for plastic behaviour of *Radiata* venners (faces) in compression, the Hill yield criterion [38] is used. Hill criterion [38] is an extended formulation of the Von-Mises yield criterion, which accounts for the anisotropy of the material. The elastic-plastic stress-strain relationship of timber in compression used in the FEA is shown in Fig. 10b. The stress potential in the Hill criterion is expressed as

$$\sigma_e = \sqrt{F_{33}\left(\sigma_x - \sigma_y\right)^2 + F_{11}\left(\sigma_y - \sigma_z\right)^2 + F_{22}\left(\sigma_z - \sigma_x\right)^2 + 2N_{12}\tau_{xy}^2 + 2N_{23}\tau_{yz}^2 + 2N_{31}\tau_{xz}^2} \qquad (24)$$

where $F_{ii}\left(i = 1,2,3\right)$ and $N_{ij}\left(i \neq \mathrm{j} = 1,2,3\right)$ are constants obtained from the material tests conducted in different orientations

$$F_{ij}=\left[\frac{(\sigma_0)^2}{2}\right]\left[\frac{1}{(\sigma_{jj}^y)^2}+\frac{1}{(\sigma_{kk}^y)^2}-\frac{1}{(\sigma_{ii}^y)^2}\right]=\frac{1}{2}\left[\frac{1}{R_{jj}{}^2}+\frac{1}{R_{kk}{}^2}-\frac{1}{R_{ii}{}^2}\right]\begin{Bmatrix} i=1,2,3 \\ j=2,3,1 \\ k=3,2,1 \end{Bmatrix} \tag{25a}$$

$$N_{ij}=\frac{3}{2}\left[\frac{(\tau_0)^2}{\sigma_{ij}^y}\right]=\frac{3}{2}\left[\frac{1}{R_{ij}{}^2}\right] \quad (i\neq j=1,2,3) \tag{25b}$$

where σ_{ii}^y and σ_{ij}^y correspond to the normal and shear yield stresses, and subscripts 1, 2 and 3, are associated with the longitudinal, tangential and radial directions, respectively. R_{ij} are the yield ratios which relate the yield level for stress components σ_{ij}^y, to the reference yield stress σ_0 of the material. The yield ratios are defined as follows:

$$R_{ij}=\begin{Bmatrix} \dfrac{\sigma_{ij}^y}{\sigma_0}, & \text{if } i=j \\ \dfrac{\sigma_{ij}^y}{\tau_0}, & \text{if } i\neq j \end{Bmatrix} \tag{26a}$$

$$\tau_0=\frac{\sigma_0}{\sqrt{3}} \tag{26b}$$

In the current study, $R_{11}=1, R_{22}=0.25, R_{33}=0.26, R_{12}=R_{13}=0.9, R_{23}=0.66$ and the reference yield stress σ_0 =18, 21 and 30 MPa with tangent modulus of E_T =345 MPa are adopted [39].

4.3 FEA results

The load vs. mid-span deflection responses of the 6 × 1 m, double layer BCS and PCS panels are shown in Fig. 11, and the stress ratios at failure and corresponding failure modes are represented in Table 5. The solid lines in Fig. 11, correspond to the Ritz method results based

on linear orthotropic material properties, and small deflection theory. The dashed lines are associated with the FEA results with different reference yield stress (σ_0). The FEA curves are stopped when the failure is reached. All the investigated panels experienced failure in tension parallel to the grain. As shown in Fig. 11, the slopes of the load-deflection responses from the Ritz method and the FEA match perfectly for deflections up to 6 mm (Δ/L =0.001). Beyond this point, the nonlinear geometric behaviour is observed in the FEA results. The contribution of the nonlinear material behaviour corresponding to the faces in compression, is only observed at very large deflections. At similar reference yield stress σ_0 =18 MPa, the material nonlinearity commences at deflections beyond 40 mm in BCS (Δ/L =0.007) and, 35 mm in the PCS panels (Δ/L =0.006), respectively. As the σ_0 value is decreased, the plateau region of the load-deflection curve prior to the ultimate load is extended. This is more evident in the BCS response, and suggests relatively more ductile behaviour in the BCS panels compared to the PCS panels.

The ultimate capacities (q_u) of the panels obtained from the FEA are represented in Table 5. The largest capacity is q_u =48.24 kPa, corresponds to the PCS panel with σ_0 =30 MPa, and is 27% larger than the capacity of the BCS panel with the same reference yield stress (σ_0). However, the PCS 21-30-9 panel is 30 % heavier than BCS 21-30-9 panel according to the weight ratios of Table 4 with $a = 6$ m and $b = 1$ m. As the σ_0 value is decreased, the ultimate capacity of the panel decreases. This drop in the ultimate capacity is more evident in the PCS panel. As represented in Table 5, at the failure point($\sigma^{22}/\sigma_{tu}^{22} = 1.0$), the panels almost reach the ultimate capacity in tension perpendicular to the grain. The largest capacities are observed in panels with the highest σ_0 =30 MPa. In these panels the face in tension fails

due to the normal stress in direction parallel to the grain exceeding the capacity, $\sigma_{tu}^{\shortparallel}$, while the face in compression has not reached the yield point.

5. Conclusions

The flexural stiffness and ultimate load capacity of novel ultralight composite sandwich panels, namely; (a) Bamboo Core Sandwich (BCS) panel, and (b) Peeling Core Sandwich (PCS) panel were investigated. A modified Ritz method was developed herein, which unlike previous formulations of sandwich orthotropic plates, accounts for the local bending stiffness of the faces (thick face) and the flexural rigidity of the cores (thick-stiff core) of the BCS and PCS panels. Results of the Ritz method were compared against predictions of a sandwich beam theory (Timoshenko beam) and were validated against published experimental results. Using the validated Ritz method, bending stiffness of the BCS and PCS panels were compared with CLT panels of almost similar depths. Ultimate capacities of the panels were obtained from FEA, which accounts for nonlinear geometric and material effects. It was understood that in one-way bending, the studied PCS panels of different lengths are in average 10% stiffer than the BCS panels. The Timoshenko beam coefficients of the BCS and PCS panels were found to be 0.817 and 0.815, respectively, which are much smaller than the coefficient 1.2 for the CLT panels. Using the validated FEA, the ultimate capacity of the 6×1 m PCS panel was found to be 27% larger than the capacity of the BCS panel. These numbers should be interpreted with regards to the 30% larger weight of the PCS compared to its counterpart BCS panel. The stiffness of BCS and PCS panels can get as high as 17% and 25% of the stiffness of the CLT panels with similar panel depths, respectively. In two-way bending (6×8 m panel), the stiffness of the BCS and PCS panels are 20% and 29% larger than the CLT at almost similar panel depth. The mentioned BCS and PCS panels are almost 40% and 20% lighter than their competitive CLT panel (*CL*7/295). The FEA results showed

that in all the studied BCS/PCS panels, failure occurred in tension parallel to the grain. Further experimental studies are planned to manufacture and test the BCS and PCS panels and to obtain the ultimate capacity and optimised geometric configuration of the cores within the panel.

References

[1] Manalo, A., Aravinthan, T., Karunasena, W., & Ticoalu, A. A review of alternative materials for replacing existing timber sleepers. Composite structures 2010; 92(3): 603-611.

[2] Liew, J. R., & Sohel, K. Structural performance of steel-concrete-steel sandwich composite structures. Advances in Structural Engineering 2010; 13(3): 453-470.

[3] Dawood, M., Taylor, E., & Rizkalla, S. Two-way bending behavior of 3-D GFRP sandwich panels with through-thickness fiber insertions. Composite structures 2010; 92(4): 950-963.

[4] Sohel, K., & Liew, J. R. Steel–Concrete–Steel sandwich slabs with lightweight core-Static performance. Engineering structures 2011; 33(3): 981-992.

[5] Grenestedt, J. L., & Bekisli, B. Analyses and preliminary tests of a balsa sandwich core with improved shear properties. International journal of mechanical sciences 2003; 45(8): 1327-1346.

[6] Mamalis, A., Spentzas, K., Manolakos, D., Ioannidis, M., & Papapostolou, D. Experimental investigation of the collapse modes and the main crushing characteristics of composite sandwich panels subjected to flexural loading. International journal of crashworthiness 2008; 13(4): 349-362.

[7] Reis, E. M., & Rizkalla, S. H. Material characteristics of 3-D FRP sandwich panels. Construction and building materials 2008; 22(6): 1009-1018.

[8] McCormack, T., Miller, R., Kesler, O., & Gibson, L. Failure of sandwich beams with metallic foam cores. International Journal of Solids and Structures 2001; 38(28): 4901-4920.

[9] Kabir, K., Vodenitcharova, T., & Hoffman, M. Response of aluminium foam-cored sandwich panels to bending load. Composites Part B: Engineering 2014; 64: 24-32.

[10] Nia, A. A., & Sadeghi, M. The effects of foam filling on compressive response of hexagonal cell aluminum honeycombs under axial loading-experimental study. Materials & Design 2010; 31(3): 1216-1230.

[11] Brandner, R., Flatscher, G., Ringhofer, A., Schickhofer, G., & Thiel, A. Cross laminated timber (CLT): overview and development. European Journal of Wood and Wood Products 2016; 74(3): 331-351.

[12] Fellmoser P, Blass HJ. Influence of rolling shear modulus on strength and stiffness of structural bonded timber elements. In: Gorlacher R, editor. CIBW18 meet., Scotland; 2004. p. 8.

[13] Styles, M., Compston, P., & Kalyanasundaram, S. The effect of core thickness on the flexural behaviour of aluminium foam sandwich structures. Composite structures 2007; 80(4): 532-538.

[14] Daniel, I. M., & Abot, J. L. Fabrication, testing and analysis of composite sandwich beams. Composites Science and Technology 2000; 60(12): 2455-2463.

[15] CoDyre, L., & Fam, A. The effect of foam core density at various slenderness ratios on axial strength of sandwich panels with glass-FRP skins. Composites Part B: Engineering 2016; 106: 129-138.

[16] Mahfuz, H., Islam, M. S., Rangari, V. K., Saha, M. C., & Jeelani, S. Response of sandwich composites with nanophased cores under flexural loading. Composites Part B: Engineering 2004; 35(6): 543-550.

[17] Tuwair, H., Hopkins, M., Volz, J., ElGawady, M. A., Mohamed, M., Chandrashekhara, K., & Birman, V. Evaluation of sandwich panels with various polyurethane foam-cores and ribs. Composites Part B: Engineering 2015; 79: 262-276.

[18] Dawood, M., Taylor, E., Ballew, W., & Rizkalla, S. Static and fatigue bending behavior of pultruded GFRP sandwich panels with through-thickness fiber insertions. Composites Part B: Engineering 2010; 41(5): 363-374.

[19] Amada S, Ichikawa Y, Munekata T, Nagase Y, Shimizu K. Fiber texture and mechanical graded structure of bamboo. Composite Part B 1997; 28:13–20.

[20] Melo, R. R. d., Menezzi, D., Soares, C. H., Pavan, B. E., & Rodolfo Júnior, F. Rotary peeling yield of Schizolobium amazonicum (Leguminosae-Caesalpinioideae). Acta Amazonica 2014; 44(3): 315-320.

[21] Allen, H. G. Analysis and design of structural sandwich panels: Pergamon Press, oxford, 1969.

[22] MATLAB R2016a release and MATHWORKS Inc., Natick, Massachusetts, USA.

[23] Timoshenko, S. and Woinowsky-krienger, S. Theory of Plates and Shells, McGraw-Hill, New York; 1959.

[24] Kreuzinger H. 1995. Mechanically jointed beams and columns. In Timber Engineering – STEP 1, ed. H. J. Blass et al., B11/1-8. Almere, The Netherlands: Centrum Hout.

[25] Gagnon, S., & Pirvu, C. CLT Handbook-Canadian Edition Chapter 3: Structural design of cross laminated timber elements. In: FPInnovations; 2011.

[26] Awad, Z. K., Aravinthan, T., Zhuge, Y., & Manalo, A. Geometry and restraint effects on the bending behaviour of the glass fibre reinforced polymer sandwich slabs under point load. Materials & Design 2013; 45: 125-134.

[27] Australian/New Zealand Standard. AS/NZS 2269.0:2012 Plywood-Structural Part 0: Specification, 2012.

[28] Ross, R. J. Wood handbook: wood as an engineering material. USDA Forest Service, Forest Products Laboratory, General Technical Report FPL-GTR-190, 2010; 509 p. 1 v., 190.

[29] Chung, K., & Yu, W. Mechanical properties of structural bamboo for bamboo scaffoldings. Engineering structures 2002; 24(4): 429-442.

[30] John A. Nairn. OSULaminates (Version version 6.0): Oregon state university, 2015.

[31] Reddy, J. A generalization of two□dimensional theories of laminated composite plates. International Journal for Numerical Methods in Biomedical Engineering 1987; 3(3): 173-180.

[32] XLam. Designing with XLam Cross Laminated Timber. New Zealand Design Guide Version 2.1; 2016.

[33] ANSYS 17.0 release. A.I., 275 Technology Drive, Canonsburg, PA 15317.

[34] Raftery, G. M., & Harte, A. M. Nonlinear numerical modelling of FRP reinforced glued laminated timber. Composites Part B: Engineering 2013; 52: 40-50.

[35] Xu BH, Taazount M, Bouchair A, Racher P. Numerical 3D finite element modelling and experimental tests for dowel-type timber joints. Constr Build Mater 2009; 23: 3043–52.

[36] Valipour, H. R., & Crews, K. Efficient finite element modelling of timber beams strengthened with bonded fibre reinforced polymers. Construction and building materials 2011; 25(8): 3291-3300.

[37] Xu, B., Bouchaïr, A., Taazount, M., & Vega, E. Numerical and experimental analyses of multiple-dowel steel-to-timber joints in tension perpendicular to grain. Engineering structures 2009; 31(10): 2357-2367.

[38] Hill R. The mathematical theory of plasticity. Oxford (NY): Oxford University Press; 1950.

[39] Alam P. The reinforcement of timber for structural applications and repair. PhD thesis. Dept. of Mech. Eng. University of Bath; 2004.

List of Figures

List of Tables

Table 4. Properties of the BCS and CLT panels and corresponding weight and stiffness ratios

Table 5. Modes of failure for BCS (21-30-9) and PCS (21-30-9) panels under one-way bending

Table 1. Material properties of bamboo, peeling cores and *Radiata* Pine used in the BCS and PCS panels

Material	E_X (MPa)	E_Y (MPa)	E_Z (MPa)	G_{XY} (MPa)	G_{YZ} (MPa)	G_{XZ} (MPa)	υ_{XY}	υ_{YZ}	υ_{XZ}	Density (kg/m^3)
Bamboo core	10,500	1,260	1,260	630	630	630	0.3	0.3	0.3	740
Peeling core	10,500	1,260	1,260	630	630	630	0.3	0.3	0.3	440
Radiata ply	15,070	678	1,115	798	150	829	0.444	0.387	0.392	590
GFRP (faces)	11,750	9,650	9,650	2,465	2,173	2,173	0.3	0.3	0.3	-

Table 2. Material properties of the BCS and PCS faces calculated from the classical laminate theory [30]

Panel ID	MOE Longitudinal (MPa)	MOE Transverse (MPa)	Shear Modulus (MPa)	Poisson's ratio (in $\boldsymbol{yx}$- plane)	Nominal thickness of individual plies through the single layer assembly (mm)
18-30-7 single layer	9,382	6,483	799	0.03	3.0/2.4/2.4/2.4/2.4/2.4/3.0
18-30-7 double layer	9,832	6,483	799	0.03	
21-30-9 single layer	11,037	4,827	799	0.06	3.0/1.5/3.0/1.5/3.0/1.5/3.0/1.5/3.0
21-30-9 double layer	11,037	4,827	799	0.06	
25-30-9 single layer	8,278	7,588	799	0.03	3.0/2.4/3.0/2.4/3.0/2.4/3.0/2.4/3.0
25-30-9 double layer	8,278	7,588	799	0.03	

Table 3. Material properties of the CLT laminations and selected panels taken from *XLam* product sheet [32]

	MOE Longitudinal (MPa)	MOE Transverse (MPa)	Shear Modulus (parallel to span) (MPa)	Shear Modulus (perpendicular to span) (MPa)
External laminations	8,000	360	440	80
Internal laminations	6,000	270	330	60
CL7/295	4,376	2,531	364	-
CL7/315	4,116	2,752	362	-

Table 4. Properties of the BCS, PCS and CLT panels and corresponding weight and stiffness ratios

Dimensions		CLT		BCS			PCS			Ratios			
a (m)	b (m)	h_{CLT} (mm)	W_{CLT} (kg/m^2)	h_{BCS} (mm)	C_{BCS} (mm)	Double layer	h_{PCS} (mm)	C_{PCS} (mm)	Double layer	$W_{(BCS)}/W_{(CLT)}$	$K_{(BCS)}/K_{(CLT)}$	$W_{(PCS)}/W_{(CLT)}$	$K_{(PCS)}/K_{(CLT)}$
4.0	1.0	295	151	284	200	21-30-9	272	200	18-30-7	0.61	1.17	0.79	1.01
6.0	1.0	295	151	284	200	21-30-9	284	200	21-30-9	0.61	1.13	0.79	1.25
7.0	1.0	315	161.2	294	210	21-30-9	284	200	21-30-9	0.58	1.06	0.74	1.07
6.0	8.0	295	151	284	200	21-30-9	272	200	18-30-7	0.61	1.20	0.79	1.29

Table 5. Modes of failure for BCS (21-30-9) and PCS (21-30-9) panels under one-way bending

Panel ID (Double layer)	σ_0 (MPa)	q_u (kPa)	$\sigma^{\parallel} / \sigma_{tu}^{\parallel}$	$\sigma^{\perp} / \sigma_{tu}^{\perp}$	σ_e / σ_0	Failure mode
BCS 21-30-9	30	38.09	1.0	0.96	0.87	Tension (Parallel)
BCS 21-30-9	21	37.49	1.0	0.96	1.01	Tension (Parallel)
BCS 21-30-9	18	34.48	1.0	0.96	1.05	Tension (Parallel)
PCS 21-30-9	30	48.24	1.0	0.94	0.87	Tension (Parallel)
PCS 21-30-9	21	47.57	1.0	0.96	1.04	Tension (Parallel)
PCS 21-30-9	18	38.39	1.0	0.98	1.07	Tension (Parallel)

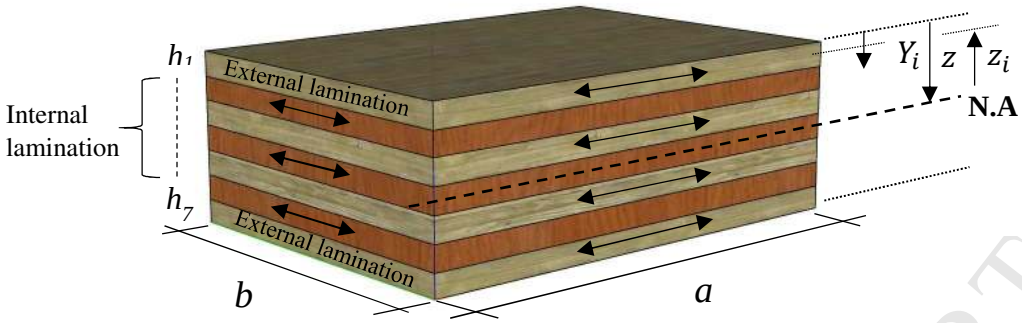

(a)

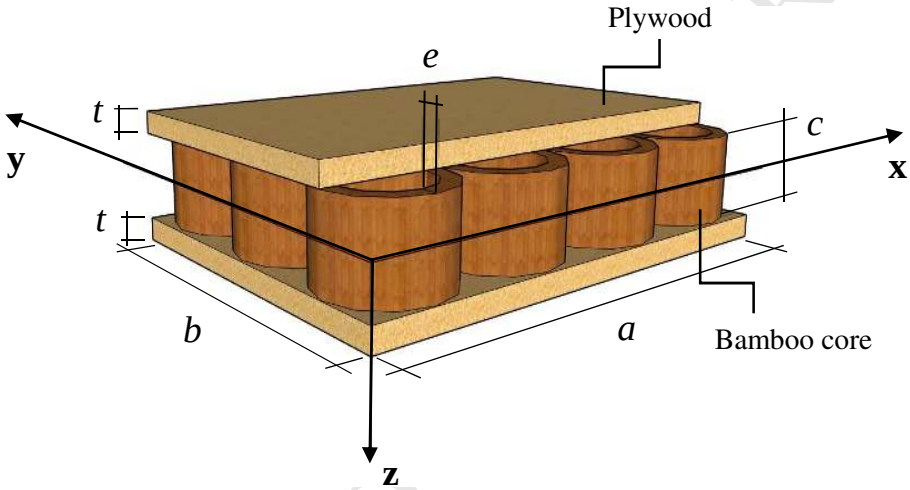

(b)

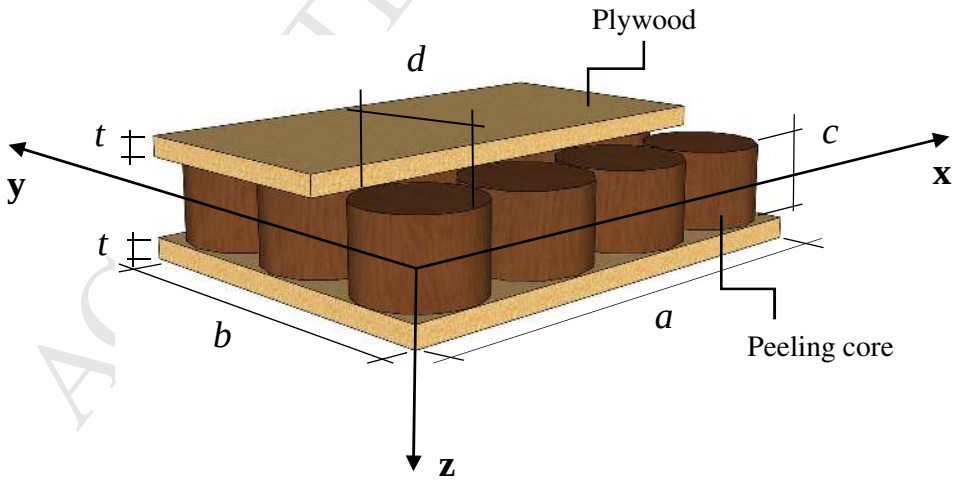

(c)

Fig. 1. A schematic illustration of (a) existing commercial Cross-laminated Timber (CLT) panel, and (b) proposed Bamboo Core Sandwich (BCS) panel and, (c) Peeling Core Sandwich (PCS) panel

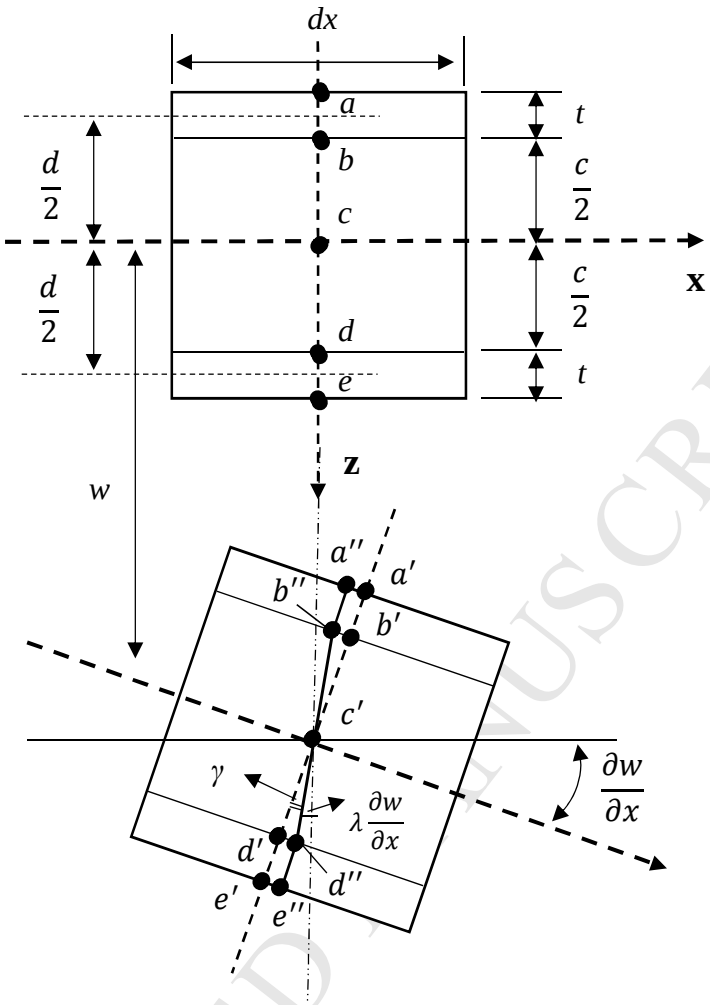

Fig. 2. Deflected shape of a short section of the BCS/PCS panel in bending, used in the Ritz method formulation

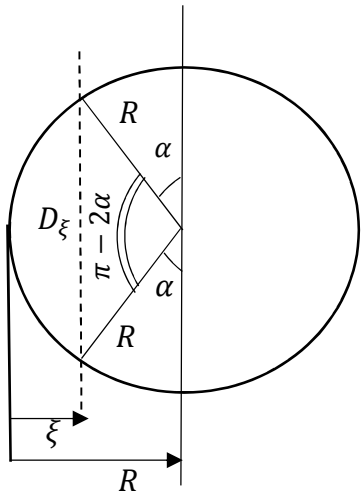

(a)

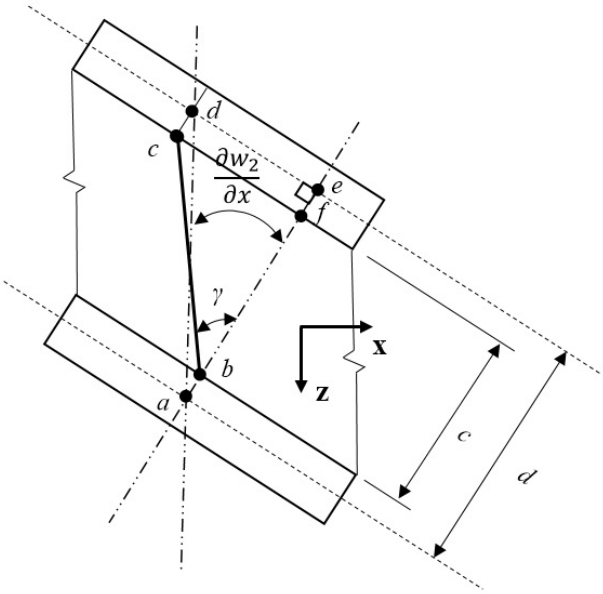

(b)

Fig. 3. (a) Cross section of a single peeling core used to find the equivalent core width (b_c) and, (b) deflected shape of a short length of the BCS/PCS panel under transverse load used in the Beam Sandwich Theory formulation

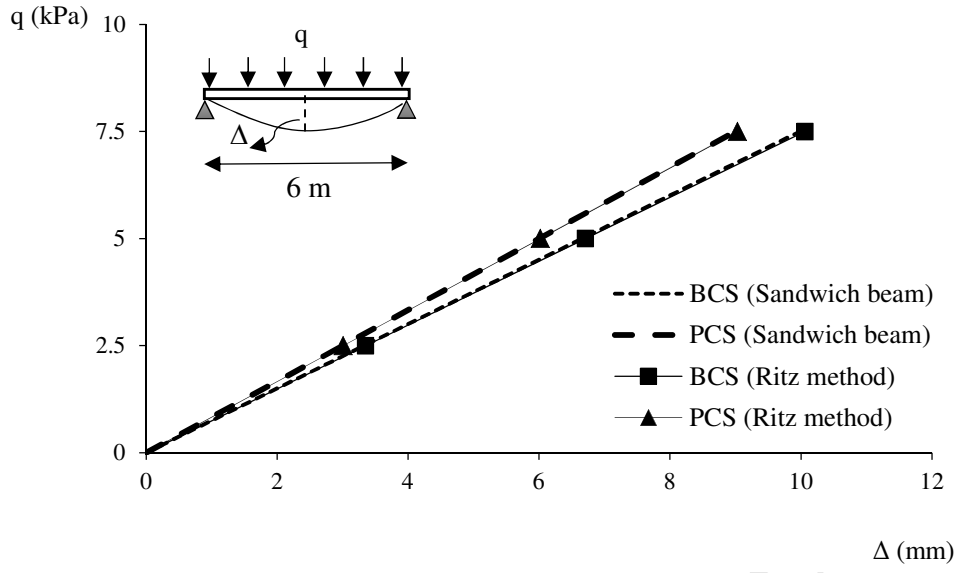

(a)

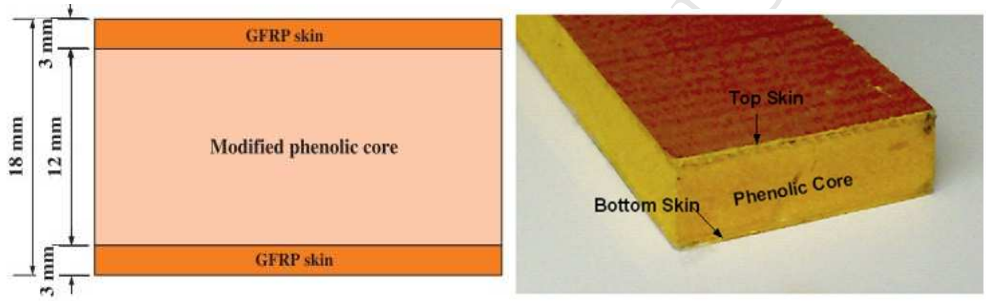

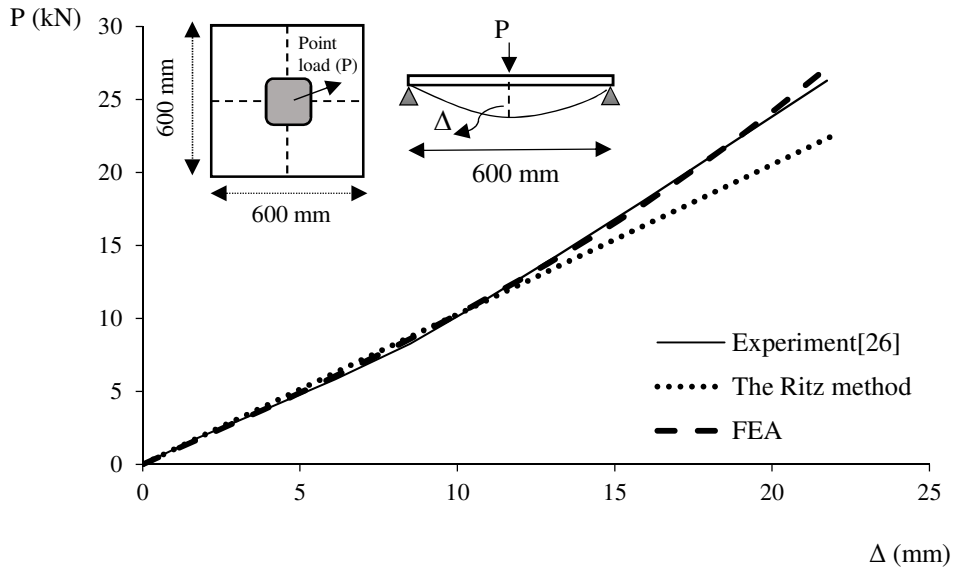

(b)

Fig. 4. (a) Load versus mid-span deflection of BCS and FCS panels using the Ritz method and the sandwich beam theory, and (b) the GFRP sandwich panel and its cross section (top), and corresponding load-deflection response of the GFRP panel from experiment [26], the proposed Ritz method and current FEA (bottom)

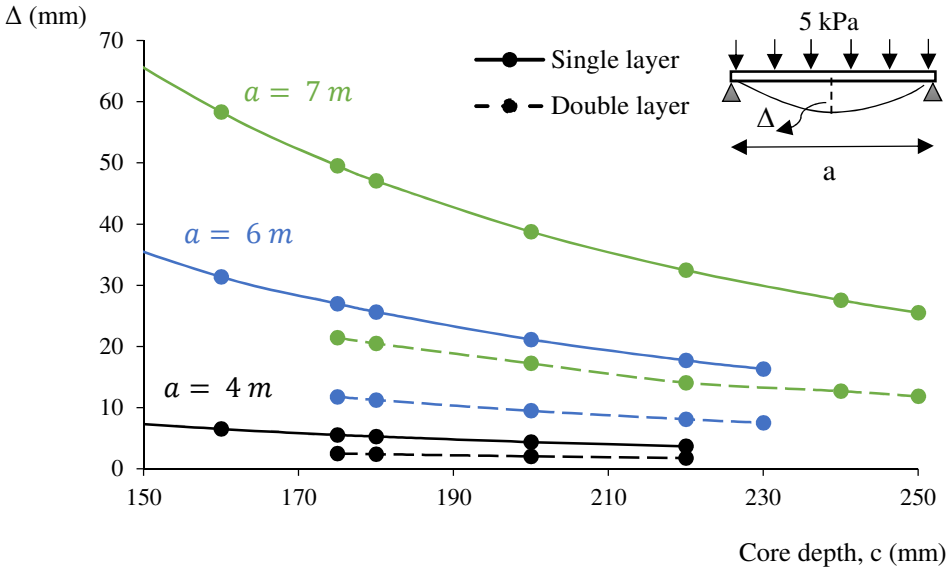

Fig. 5. Mid-span deflection of single and double layer BCS 18-30-7 narrow panels in one-way bending

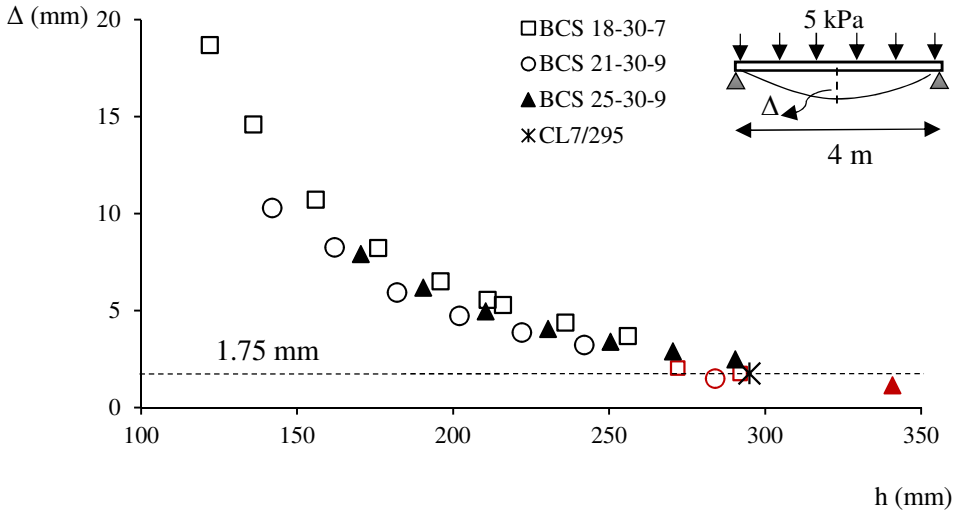

(a)

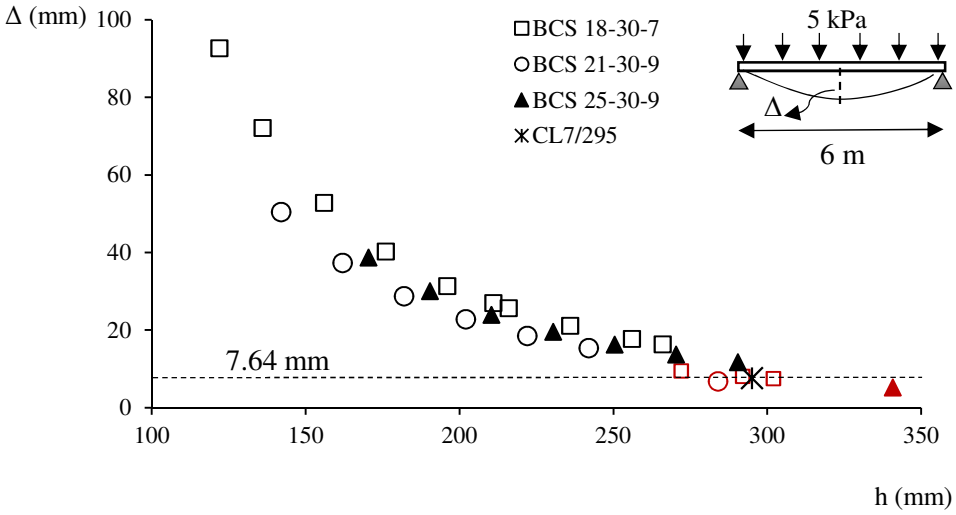

(b)

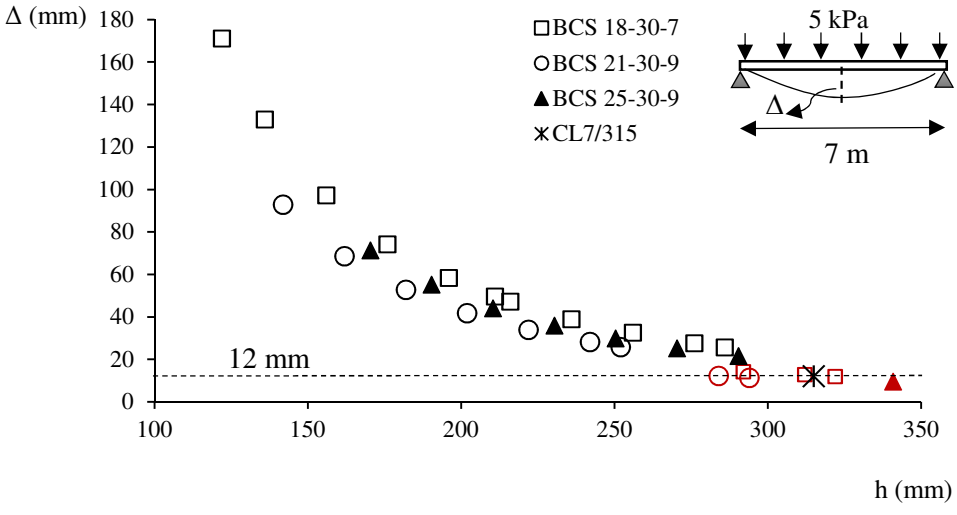

(c)

Fig. 6. Maximum deflection of BCS and CLT panels in one-way bending, (a) 4 m span, (b) 6 m span and, (c) 7 m span

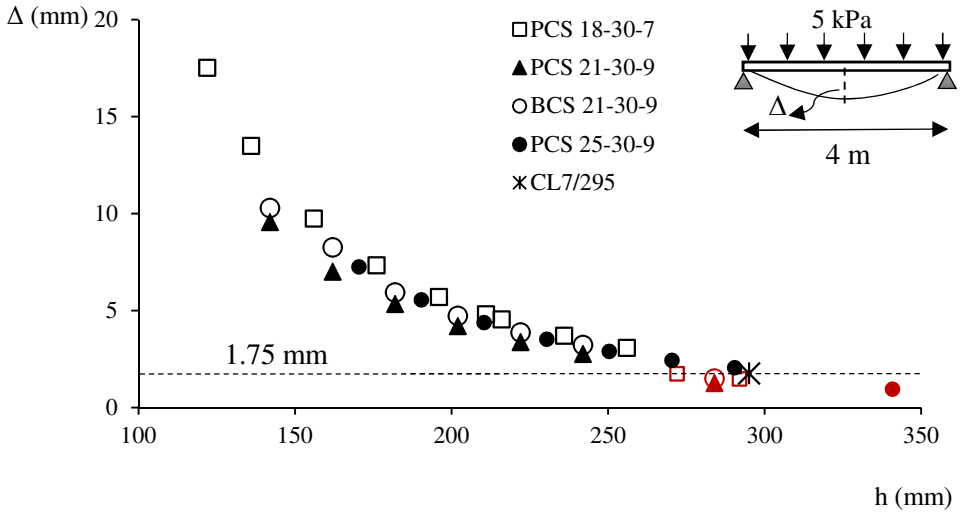

(a)

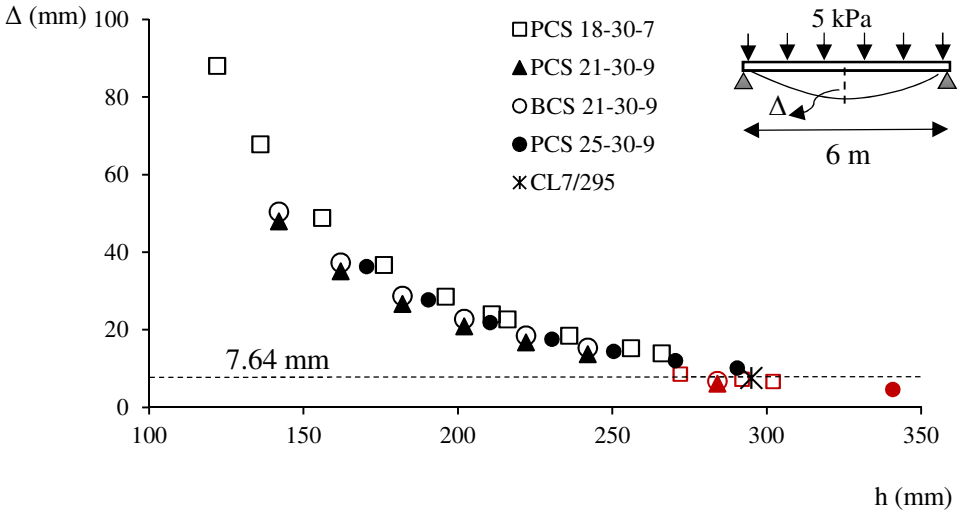

(b)

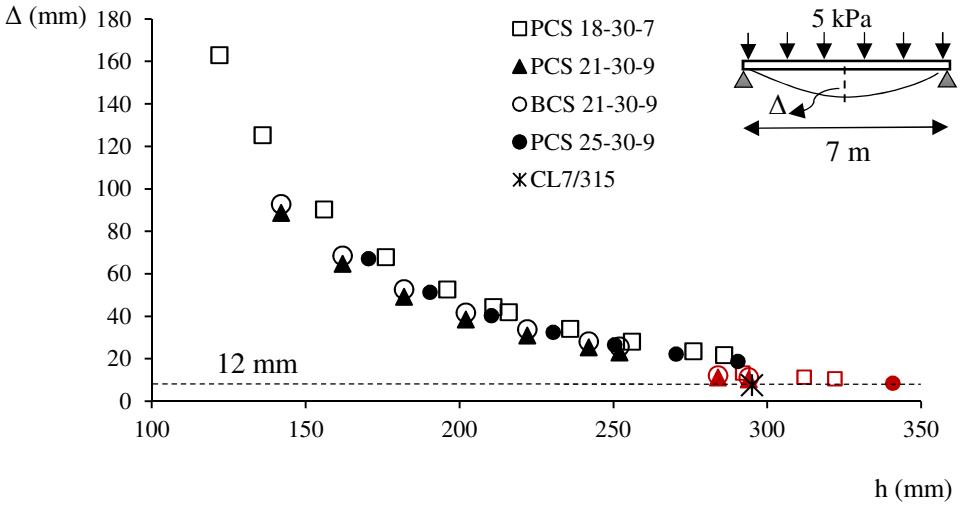

(c)

Fig. 7. Maximum deflection of BCS, PCS and CLT panels in one-way bending, (a) 4 m span, (b) 6 m span and, (c) 7 m span

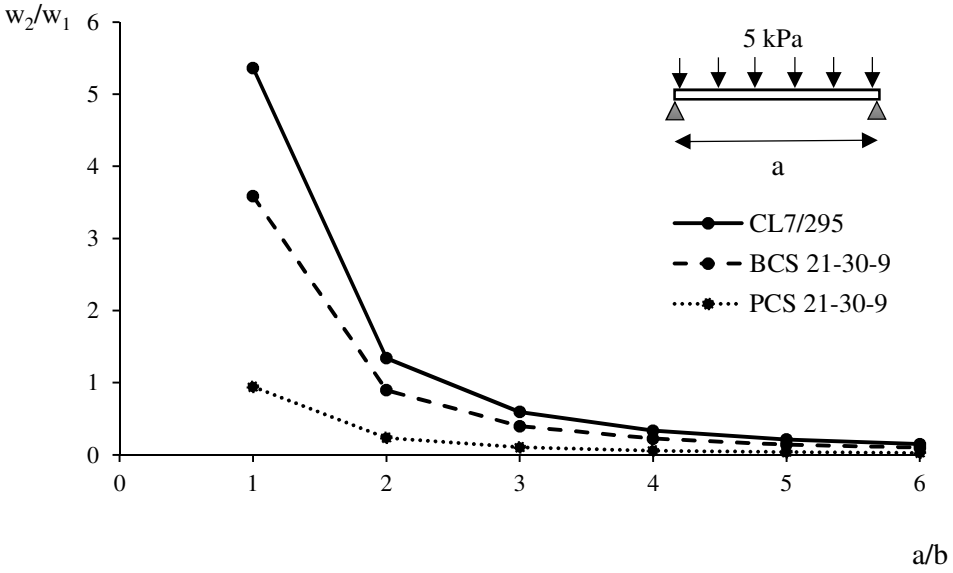

Fig. 8. The contribution of shear (w_2) and flexure (w_1) components, in the total deflection of the BCS, PCS and CLT panels in one-way bending.

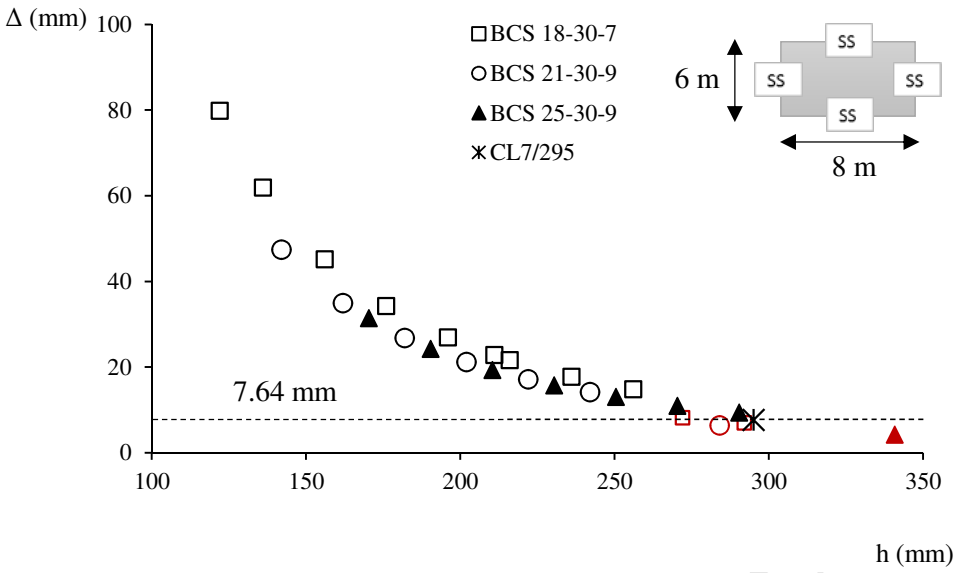

(a)

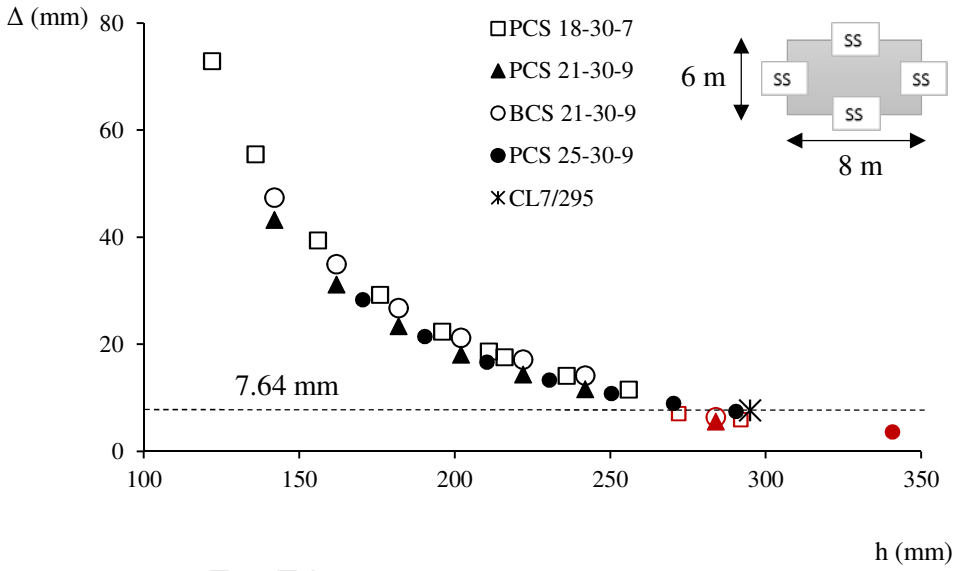

(b)

Fig. 9. Maximum deflection of BCS, PCS and CLT panels in two-way bending

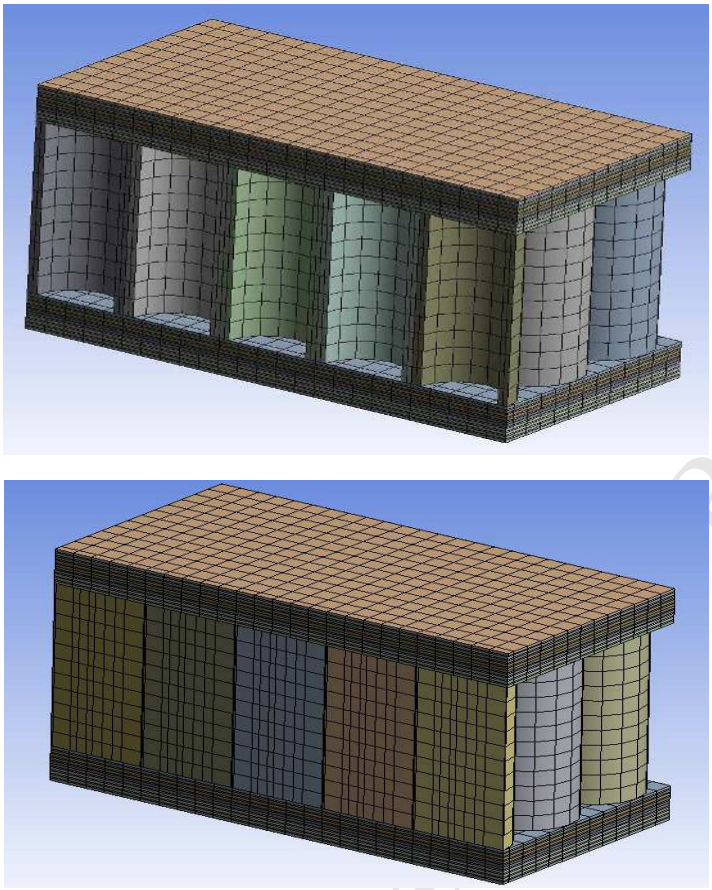

(a)

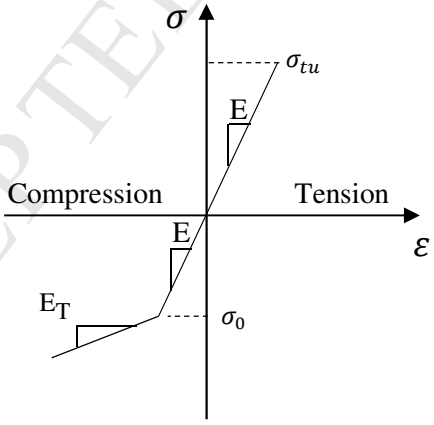

(b)

Fig. 10. A schematic illustration of (a) the FEA mesh of short section of BCS (top) and PCS (bottom) panels, (b) the adopted stress-strain relationship in the faces of the BCS/PCS panels

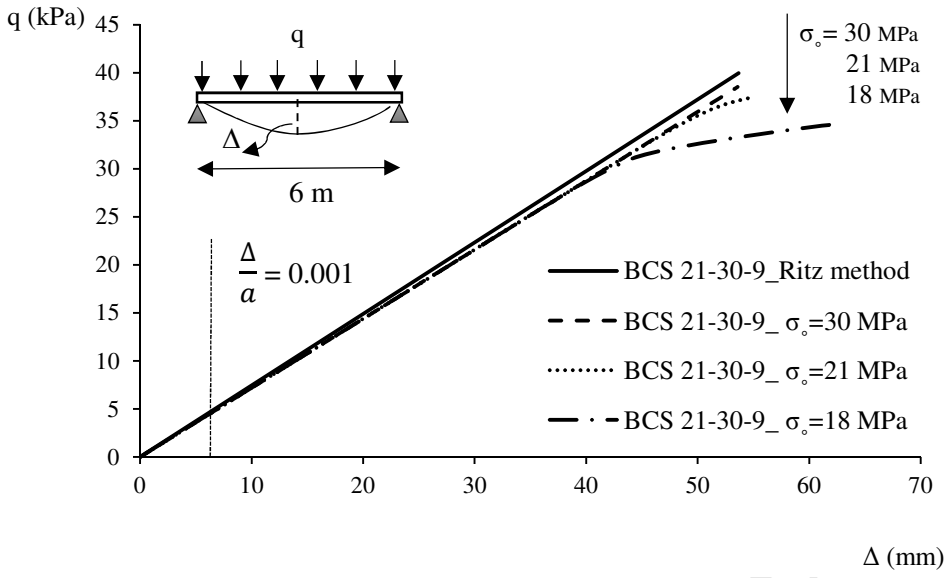

(a)

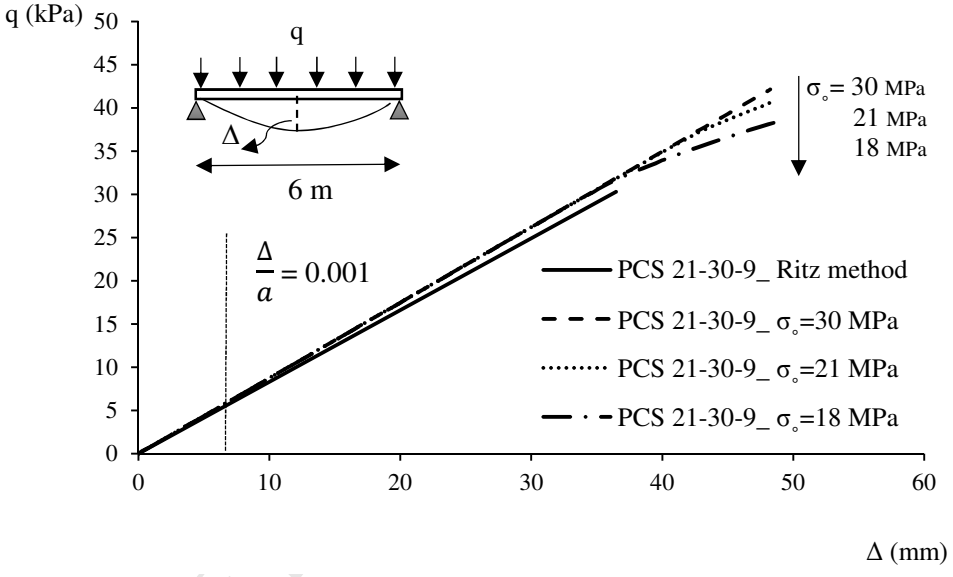

(b)

Fig. 11. The load vs. mid span deflection response of 6×1 m, (a) double layer BCS 21-30-9 and, (b) double layer PCS panels, showing the Ritz prediction, and FEA for different reference compressive yield stresses ($\sigma_\circ$)

Accepted Manuscript

Numerical study on the flexural capacity of ultra-light composite timber sandwich panels

Siavash Darzi, Hassan Karampour, Benoit P. Gilbert, Henri Bailleres

PII: S1359-8368(18)32110-3

DOI: 10.1016/j.compositesb.2018.08.022

Reference: JCOMB 5852

To appear in: *Composites Part B*

Received Date: 5 July 2018

Accepted Date: 6 August 2018

Please cite this article as: Darzi S, Karampour H, Gilbert BP, Bailleres H, Numerical study on the flexural capacity of ultra-light composite timber sandwich panels, *Composites Part B* (2018), doi: 10.1016/j.compositesb.2018.08.022.